Nano Energy 58 (2019) 852–861

Contents lists available at ScienceDirect

Nano Energy

journal homepage: www.elsevier.com/locate/nanoen

Full paper

Elastic Cu@PPy sponge for hybrid device with energy conversion and storage

Zhe Li[a,b,1], Kuan Hu[a,b,e,1], Mengyan Yang[c,1], Yang Zou[a,b,1], Jinbin Yang[c], Min Yu[a], Huaying Wang[a,b], Xuecheng Qu[a,b], Puchuan Tan[a,b], Chan Wang[a,b], Xuechang Zhou[c,*], Zhou Li[a,b,d,**]

[a] CAS Center for Excellence in Nanoscience, Beijing Key Laboratory of Micro-nano Energy and Sensor, Beijing Institute of Nanoenergy and Nanosystems, Chinese Academy of Sciences, Beijing 100083, PR China
[b] School of Nanoscience and Technology, University of Chinese Academy of Sciences, Beijing 100049, PR China
[c] College of Chemistry and Environmental Engineering, Shenzhen University, Shenzhen 518060, PR China
[d] Center on Nanoenergy Research, School of Physical Science and Technology, Guangxi University, Nanning 530004, PR China
[e] National Institute of Radiological Sciences, National Institutes for Quantum and Radiological Science and Technology, Chiba 263-8555, Japan

ARTICLE INFO

Keywords:
Sponge
Flexible
Polypyrrole
Triboelectric nanogenerator
Supercapacitor

ABSTRACT

Elastic and electrical conductive sponges are attracting materials for energy storage and energy harvest devices. In this study, we have demonstrated that a flexible and durable Cu doped PDMS sponge (Cu) can be adopted as electrodes for triboelectric nanogenerators (TENG) and flexible supercapacitors (SC). The Cu sponge loading with polypyrrole (PPy) was newly applied as single-electrode TENG for the first time. The outputs of the TENG were tuned by varying the PPy content or by combining with PDMS sponge. Due to the feasibility of changing the PPy content in the Cu@PPy sponges, this study offers a facile way to enhance the performance of TENG from the material itself with a tunable manner. Moreover, this study potentiates a better understanding of the triboelectricity produced by the TENG from the view of materials. The Cu@PPy sponges were further utilized as electrodes for all solid-state symmetrical SCs, in which the Cu sponge and PPy showed a synergistic effect on promoting the stability and performance of the SC. The SC exhibits lightweight, good capacitance, high flexibility, excellent mechanical and long-term stability, which is suitable for wearable energy storage devices. For the application of the TENG and the SC, a self-powered hybrid device was assembled, which provides a prospect for integrated devices. As a summary, we reported a new metal sponge based TENG and self-powered hybrid device, which demonstrated our study provides new opportunities for elastic multifunctional power sources and potential applications in wearable electronics.

1. Introduction

Sponge is a kind of material which features amounts of micron-to-millimeter sized pores, whilst displays intriguing mechanic properties, such as foldable, rollable, and shapeable. The modified sponges have been widely applied in energy storage, sensors, photocatalysis and other fields, to name a few [1–4]. Currently researched sponges divide into two major categories. One kind is based on three dimensional-interconnected structures, such as graphene and metal foam-based sponges [5,6]. Another kind is made of elastic polymers, such as polydimethylsiloxane (PDMS) and polyurethane (PU) sponges [7,8]. Among above-mentioned sponges, PDMS-based sponges possess numerous advantages, which hold great potential in fabricating flexible electronics, such as sensors [9,10]. Firstly, the PDMS is low-cost, simple conduction and accessible in ordinary laboratories. Secondly, the PDMS has strong adhesiveness and chemical inertly. Moreover, the PDMS sponge is readily modifiable and tailorable for variable applications. For instance, Zhou et al. recently reported a convenient method for fabricating PDMS-metal based conductive composite sponge [11]. The as-fabricated Cu@PDMS sponges (Cu sponge) exhibited splendid mechanical durability, electrical conductivity, and flexibility, which hold great potential for elastic electronics.

* Corresponding author.
** Corresponding author at: CAS Center for Excellence in Nanoscience, Beijing Key Laboratory of Micro-nano Energy and Sensor, Beijing Institute of Nanoenergy and Nanosystems, Chinese Academy of Sciences, Beijing 100083, PR China.
E-mail addresses: zli@binn.cas.cn (X. Zhou), xczhou@szu.edu.cn (Z. Li).
[1] These authors contributed equally to this work.

https://doi.org/10.1016/j.nanoen.2018.11.093
Received 18 September 2018; Received in revised form 9 November 2018; Accepted 26 November 2018
Available online 04 February 2019
2211-2855/

Particularly, with the fast development of energy harvesting technique, the triboelectric nanogenerator (TENG), which is a powerful technique with low-cost, high efficiency, and environmentally friendly features, has been used to convert almost all forms of mechanical energy in our living/working environment into electricity [12–14]. PDMS is the most commonly used tribo-material owing to its high electronegativity, flexibility, transparency, and cost effectiveness. In addition, a pattern on surface or inner structures of PDMS is readily accessible. In most previous studies, micropatterned pyramid array, nanoporous/nanowire structure, and chemical functional groups were applied to modify the tribo-material in order to obtain high surface charge density [15,16]. Recently, reports on the whole PDMS modification instead of only surface functionalization were documented, such as PDMS-based composites formation and filling with dielectric material, in which affirmed the importance of whole PDMS modification on improving the TENG output [17].

Flexible supercapacitors (SCs) are distinctly important because of their higher power density, longer cycle life, and higher charge/discharge rates as compared with those of traditional batteries [18,19]. Moreover, the flexible supercapacitors may adjust their conformations to accommodate the environmental variations while without remarkable loss in their electrochemical performance. In order to fabricate flexible supercapacitors, strain-tolerant electrodes with outstanding mechanical elasticity, high capacitance, and good durability are largely unmet and still intensely pursued [20,21].

PPy, as an electroconductive polymer (ECP) with high conductivity, good environmental stability, and high theoretical gravimetric pseudocapacitance, has been widely applied in flexible supercapacitors [22,23]. However, the conjugated PPy polymers are normally nonporous and not durable due to the decomposition after a number of charge-discharge cycles because of the swelling and shrinkage of linear macromolecular structures [24]. Kinds of templating strategies or nanostructured supporting frameworks have been developed to enhance the cycling stability of PPy and their specific capacitance [25,26]. In this context, inspired by the multiplex advantages of PDMS-based sponges mentioned above, we envisaged that the PDMS sponge may serve as a free-standing, self-supporting framework for PPy to improve its cyclability.

In terms of the inherent elasticity, good electrical conductivity, and giant surface-volume ratio of the Cu sponge, it is deemed as a good candidate material for fabricating triboelectric nanogenerators and sponge-like supercapacitors. Here we demonstrated the successful fabrication of Cu sponge-based triboelectric nanogenerators and elastic supercapacitors. Firstly, we fabricated single electrode TENGs, in which the voltage outputs were tuned by varying the PPy content in the sponge. Moreover, we demonstrated that a composite structural TENG by combining of Cu@PPy sponge with PDMS sponge further amplified the output performance. These results facilitate the understanding of triboelectric charge accumulation from the view of materials and the structure of the TENG. After that, the Cu@PPy sponge supercapacitors were devised in which the Cu sponge supplied as a three dimensional-framework and the electric conductive PPy as a coating shell for energy storage, as illustrated in Fig. 1A. The PPy and Cu sponge revealed synergistic effects on promoting the electrochemical performance of the SC. What's more, we demonstrated the Cu@PPy TENG can act as a power source for charging the Cu@PPy SC. Our study affords new opportunities for fabricating elastic energy harvesting-storage package in future.

2. Experimental section

2.1. Materials

Sugar cubes are commercial products and bought from Tai Gang Food Co., Ltd (Shenzhen, China). The average size of length, width and height are 20 ± 0.5 mm, 18 ± 0.5 mm, and 10 ± 0.5 mm, respectively. 2-Methoxyethanol, Ammonium tetrachloropalladate (II) ($(NH_4)_2PdCl_4$), vinyltrimethoxysilane (VTMS), 2-(methacryloyloxy) ethyl trimethylammoniumchlo-ride (METAC, 80 wt% aqueous solution) and all other chemicals were purchased from Sigma-Aldrich. PDMS prepolymer (Sylgard 184) and curing agent were purchased from Dow Corning.

2.2. Synthesis of Cu sponges

Referring to the previous work on the fabrication of sponges, the PDMS sponges were fabricated by the polymerization of the PDMS prepolymer and a curing agent using sugar cubes as the hard templates. PDMS sponges were first treated with air plasma for 5 min and followed by coating a layer of VTMS via silanization. The resultant VTMS-PDMS sponges were then treated with polymerization solutions containing METAC monomer and potassium persulfate (KPS) initiator for a certain time, leading to the formation of PMETAC-modified PDMS sponges. The polymer brushes played an important role in the next step of ion exchange and electroless deposition. The as-prepared PMETAC-PDMS sponges were then placed in $(NH_4)_2PdCl_4$ aqueous solution to immobilize $PdCl_4^{2-}$ by ion exchange, followed by rinsing with DI water. Finally, Cu sponge was fabricated by using the electroless metal deposition in a plating bath.

2.3. Fabrication of Cu@PPy sponges

The electropolymerization of PPy was performed in a three-electrode electrochemical workstation (CHI6601 instruments, Shanghai, China). The PPy/KNO_3 mixed solution was applied as the electrolyte. The concentration of PPy is 0.1 M and the concentration of KNO_3 is 1.0 M. The as-grown bulk Cu sponges with a size of 1.5 cm × 1.5 cm × 1.0 cm were used as the working electrodes. A Pt sheet and Ag/AgCl were used as the counter and reference electrodes, respectively. The electrodeposition was proceeded for 50,100,150 and 200 cycles under a voltage window of −0.5 to 0.2 V. The PPy monomers were adsorbed on the surface of Cu sponge. After the electrodeposition process, the crosslinked Cu@PPy sponges were rinsed with distilled water and then dried to measure the qualities.

2.4. Material characterization

The sample morphology and structure were characterized using scanning electron microscope (SEM, SU8020). X-ray diffraction (XRD) study was performed using PANalytical X'Pert3 Powder with CuKα radiation (λ = 1.5406 Å). XRD pattern were recorded ranging from 5° to 100° and operating at 40 kV and 40 mA. Fourier transform infrared spectroscopy (FTIR spectra) were recorded on a FT-IR system (Bruker/VERTEX80v).

2.5. Fabrication and characterization of S-TENG

The single electrode sponge based TENG was fabricated using as-prepared Cu or Cu@PPy sponge. A piece of Cu wire was insert into the inner of sponge with conducted silver paste for fixation. Moreover, the Cu@PPy + PDMS sponge based TENG was produced by one piece of PDMS sponge, one Cu@PPy sponge and only one conductor connected to Cu@PPy sponge. As PDMS mixed with cross-linking agent by 10:1, a little mixture was placed between the two sponges. Once the PDMS cured, they are able to adhere to each other. The output was measured with an electrometer (Keithley 6517B). The frequency applied on TENGs by hand was 1 Hz and the operating distance is 10 cm.

2.6. Measurement to S-TENG

The frequency applied on TENGs by hand was 1 Hz and the operating distance is 10 cm. When the sponge SC was charged by S-TENG,

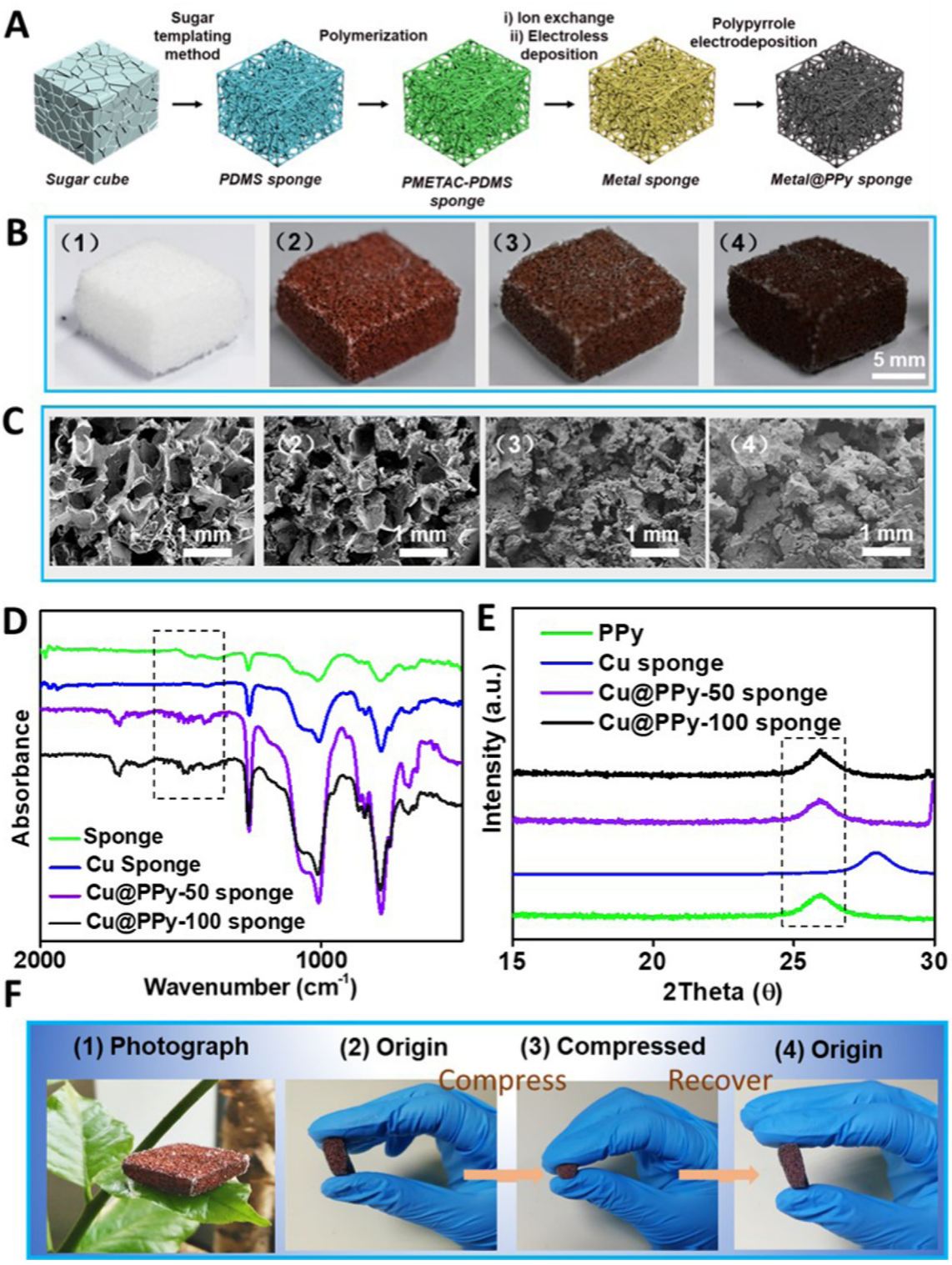

Fig. 1. Fabrication and Characterization of Cu sponges. (A) By templating method and electrodeposition, Metal@PPy sponges (Cu@PPy sponges) were prepared. (B) Pictures of sponges. (1) PDMS sponge; (2) Cu sponge; (3) Cu@PPy-50 sponge; (4) Cu@PPy-100 sponge. (C) Morphology of sponges determined by SEM. (1) PDMS sponge; (2) Cu sponge; (3) Cu@PPy-50 sponge; (4) Cu@PPy-100 sponge. (D) FTIR spectra of Cu@PPy sponges. (E) X-ray diffraction pattern of PPy modified Cu sponges. (F) Physical map of Cu sponge. (1) Cu sponge; (2) Initial state of Cu sponge; (3) The Cu sponge was compressed; (4) Recovered to the initial state.

the linear motor was employed. The open circuit voltage, short circuit current and transferred quantity of S-TENG were measured and recorded with an electrometer (Keithley 6517B), respectively.

2.7. Preparation of the PVA/KOH electrolyte

3 g PVA was dissolved in 30 mL deionized water while heating in 90 °C water bath with continuous stirring until the transparent solution was obtained. 3 g KOH was added to 30 mL deionized water under constantly stirring. After the PVA gel solution cooled to the room

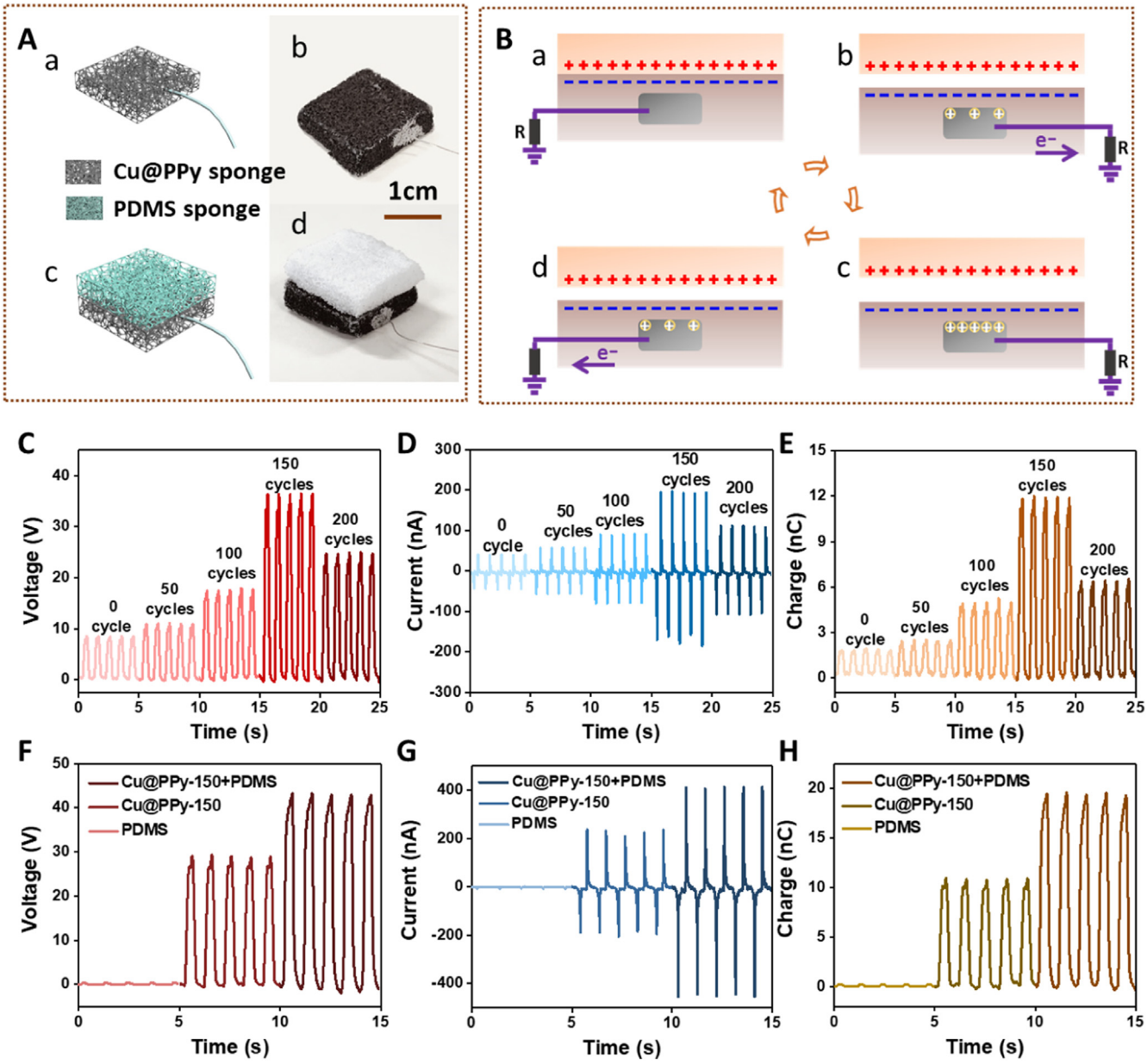

Fig. 2. Fabrication of sponge based TENG. (A) Diagram and photograph of sponge TENG. (B) Schematic working mechanism of the S-TENG. (C-E) The output voltages, current curves, and charge quantities of the sponge TENG with different PPy depositions, respectively. (F-H) The output voltages, current curves and charge quantities of the sponge TENG, respectively.

temperature, the KOH solution was dropped into under continuous stirring until the clear solution was obtained.

2.8. Preparation of all-solid-state symmetric supercapacitors

Two slices of Cu@PPy-100 sponges with the size of 1.5 cm × 1.5 cm × 1.0 cm, acted as the cathode and anode. They were coated with a thin layer of PVA/KOH electrolyte and assembled face to face through gentle squeezing under room temperature. Then the SC was wrapped with a poly(vinyl chloride) film. Finally, the all-solid-state symmetric supercapacitor was assembled, termed as Cu@PPy// Cu@PPy.

2.9. Electrochemical measurements

The electrochemical properties of the capacitor cell including cycling voltammetry curve (CV), galvanostatic charge/discharge (C/D) and electrochemical impedance spectroscopy (EIS) were measured using a CHI6601 electrochemical workstation. The CV curves were measured under different scan rates from 0.1 to 10 V s^{-1} between 0 and 0.8 V. EIS measurements were carried out in the frequency range from 100 kHz to 0.01 Hz at open circuit potential with an AC perturbation of 5 mV. Electrochemical measurements were carried out in a 1.0 M KOH aqueous electrolyte at room temperature. The mass capacitance of the supercapacitor was calculated from the CV or C/D curves according to the equations (1) and (2). The SCs were compressed under different strain. When the sponges were compressed by 10%, 30% and 50%, the corresponding CV curves were measured. We also measured the CV curves under different bending states. The bending angles are 30°, 90°, 120°and 180°.

2.10. Integrating TENG with supercapacitor

Sponge based TENG, rectifier, all-solid symmetric supercapacitor device and switch were connected in series. A LED light were parallel

connected to the SCs. When the switch was off, the SCs were charged with sponge based TENG while the switch is on, the led were lighted by SCs with full power.

3. Result and discussion

The Cu sponges were prepared by using the methods described previously [27]. As shown in Fig. 1A, the as-fabricated Cu sponges are porous, which displayed approximately 1.5 cm × 1.5 cm × 1.0 cm in size. To obtain the Cu@PPy sponge, the PPy was transferred to the Cu sponge by using a reported electrochemical deposition method [28]. With the accumulation of deposition cycles, the Cu sponges gradually turned into dark brown (Fig. 1B and S1A), which indicated the PPy loaded onto the Cu sponge indeed. Besides, Cu@PPy sponges maintain their original structure, which suggested that the deposition process has no damage to the structure of the sponges. The morphology of sponge and its derivatives were firstly characterized by scanning electron microscopy (SEM) [29]. From Fig. 1C, the PDMS sponge is poriferous at first and after Cu particles decoration, the pores' size in PDMS sponge was reduced. When the PPy electrodeposition was performed, the pores of PDMS@Cu sponge were filled with small pieces of PPy nanosheets. Notably, these PPy nanosheets were closely bound to the Cu particles and formed Cu@PPy core-shell structures in local (Fig. 1B and S1). To further probe the structure of PPy on the Cu sponges, Fourier Transform Infrared Spectroscopy (FTIR) spectroscopy characterization was conducted. The bands at 1548 and 1476 cm^{-1} could be ascribed to C=C and C-N asymmetric and symmetric stretching vibration of the pyrrole ring, as labels in Fig. 1D (dashed line). Fig. 1E showed the X-ray diffraction (XRD) pattern of Cu sponges and Cu@PPy sponges. A polarization peak around $2\theta = 26^{\circ}$ was observed, which is an indicator for the amorphous structure to PPy. The final Cu@PPy sponge was ultralight weight and could be supported by a leaf. For a 1.5 cm × 1.5 cm × 1.0 cm sized Cu@PPy sponge, the total mass is less than one gram. The striking low mass density of the sponge enable its rather attracting for flexible electrode uses. Significantly, the fabricated Cu sponge possesses intriguing elasticity, which can be compressed to half of its initial thickness and recovered without any deformation. (Fig. 1F).

Triboelectric nanogenerator is a new type of energy harvester and received widespread attention [30,31]. In this study, we devised the single-electrode-TENG (S-TENG), which was consisted of single Cu sponge or Cu sponge combined with PDMS sponge, as schemed in Fig. 2A. The Cu wire was connected to the inner of the Cu sponge (Cu sponge). The photograph of the as-fabricated S-TENG was shown as Fig. 2A-c, d. The proposed mechanism for electricity generation of Cu S-TENG is schematically exhibited in Fig. 2B. Firstly, the skin or pure PDMS sponge is in full contact with the surface of Cu sponge. Owing to dramatically triboelectrically positive of the human skin than PDMS, electrons will be transferred from skin into PDMS sponge, which generates positive charges on the surface of skin and negative charges on the surface of PDMS sponge (Fig. 2B-a). At this moment, the produced two kinds of triboelectric charges with opposite polarities are fully balanced, so without electron flowing in the external circuit. As the skin separates from PDMS sponge, these triboelectric charges cannot be equilibrated. The negative charges on the surface of the PDMS sponge induced positive charges on the Cu electrode to reach an electrical equilibrium state, which drives electrons to flow from Cu electrode to the ground, producing an output current signal (Fig. 2B-b). When PDMS sponge and the skin getting away from each other, the negative charges on the surface of the PDMS sponge are fully sheltered from the induced positive charges on the Cu electrode without output signals (Fig. 2B-c). Moreover, as the distance between PDMS sponge and the skin become smaller, the opposite electric potential will appear. The induced positive charges on the Cu electrode will decrease. Thus, electrons will flow from ground to Cu electrode, as shown in Fig. 2B-d, resulting in a reversed output current signal. This is one cycle of single-electrode mode operation. The different PPy deposited Cu sponges were measured in our experiment to optimize the output of the S-TENG. Fig. 2C, D and E exhibit the open-circuit voltage, shortcircuit current and transferred charge quantity of the S-TENG under the oscillation frequency of 1 Hz, respectively. The deposition cycles were arranged from 0 to 200, with the corresponding unit sediment (micrograms per cubic centimeter) were 0, 125, 200, 350 and 600 μg cm^{-3}. As results, the maximum performance was achieved at the deposition cycle of 150, where the output voltage reached 29.3 V, with the associated current is 227 nA and the transferred charge is near to 12 nC. In order to further improve the output, we envisaged that the combination electrode structure of Cu and PDMS sponge would be a feasible approach due to perfectly integrating the electronegativity of the PDMS sponge and the superior conductivity of the Cu@PPy Sponge. As expected, the output of Cu@PPy-150 + PDMS sponge electrode was nearly doubled over the Cu@PPy-150 sponge TENG. The average peak values of voltage, current and charge reached about 50 V, 400 nA and 20 nC, respectively. These results demonstrated the feasibility and accessibility in fabricating of metal sponge- based elastic TENG. What's more, the considerable output of the TENG endows them potential choices for wearable energy serve package applications in the future.

Have demonstrated the great potential of Cu@PPy sponge in TENG, we wondered to explore the electrochemical properties of Cu@PPy as supercapacitors. First, we investigated whether the PPy deposition can enlarge the electrochemical performance of the sponge electrode. The electrochemical performance of Cu sponge and Cu@PPy-50 sponge electrodes were first investigated using a three-electrode system in 1.0 M KNO_3 solution electrolyte in the voltage window of −0.7 to 0 V. As shown in Fig. S2A, the Cu@PPy sponge-50 displayed apparent larger specific capacitance in contrast to Cu sponge. Besides, the Cu@PPy-50 sponge retained 96.3% of its original capacitance while the Cu sponge retained only about 70% of its initial capacitance after 5000 charging/discharging cycles (Fig. S2B), which implied that the Cu@PPy sponge-50 sponge has a dramatically superior cycling stability than Cu sponge. The weak cycling ability of Cu sponge may be attributed to the irreversible transformation of Cu(0) to Cu(I/II) species during the redox process [32,33].

According to the references, the electrochemical performance of the electrodes is closely related to the morphology of the electrodes (yet mean the thickness of the PPy on Cu sponge in our case) and the electrolytes used [34,35]. To figure out the relationship between deposition cycles and specific capacitance of the sponge electrode, we set up four groups of Cu@PPy sponge , namely Cu@PPy-50, Cu@PPy-100, Cu@PPy-150, and Cu@PPy-200, the numbers 50, 100, 150, and 200 indicate the deposition cycles applied respectively. Due to the electrolytes play a pivotal role in determining the capacitance of electrodes, we first explored the electrochemical performance of sponge electrodes in different electrolyte (1.0 M KNO_3 and 1.0 M KOH). Apparently, the sponges showed superior ion storage capacity in alkali KOH electrolyte (Fig. S3A) in compared with those in KNO_3 electrolyte, which was consistent with previous reports [36,37]. Therefore, we chose KOH as the electrolyte in all the following studies. Next, we studied the influence of deposition cycles on the electrochemical performance of Cu@PPy electrodes. The CV curves of five kinds of Cu@PPy electrodes with different deposition cycles (0, 50, 100, 150 and 200 cycles) were shown in Fig. 3A. The calculating gravimetric capacitances in KOH or KNO_3 electrolytes based on the CV curves against different deposition cycle numbers were plotted in Fig. S3B and S4A, respectively [38]. Obviously, the specific capacitances of electrodes firstly increased and then decreased along with the cycles increase. The maximum mass capacitance was achieved at 100 cycles, then the capacitances tended to keep stable from 100 to 200 cycles. Electrochemical impedance spectroscopies (EIS) of the Cu@PPy, Cu@PPy-50, and Cu@PPy-100 sponges were tested and their Nyquist plots were shown in Fig. 3B and S4. All spectra displayed a semicircle in the high frequency range and a sloping line in the low frequency range. The equivalent series resistance (*Rs*) was read at the intercept of the semicircle on the Z′ axis at high

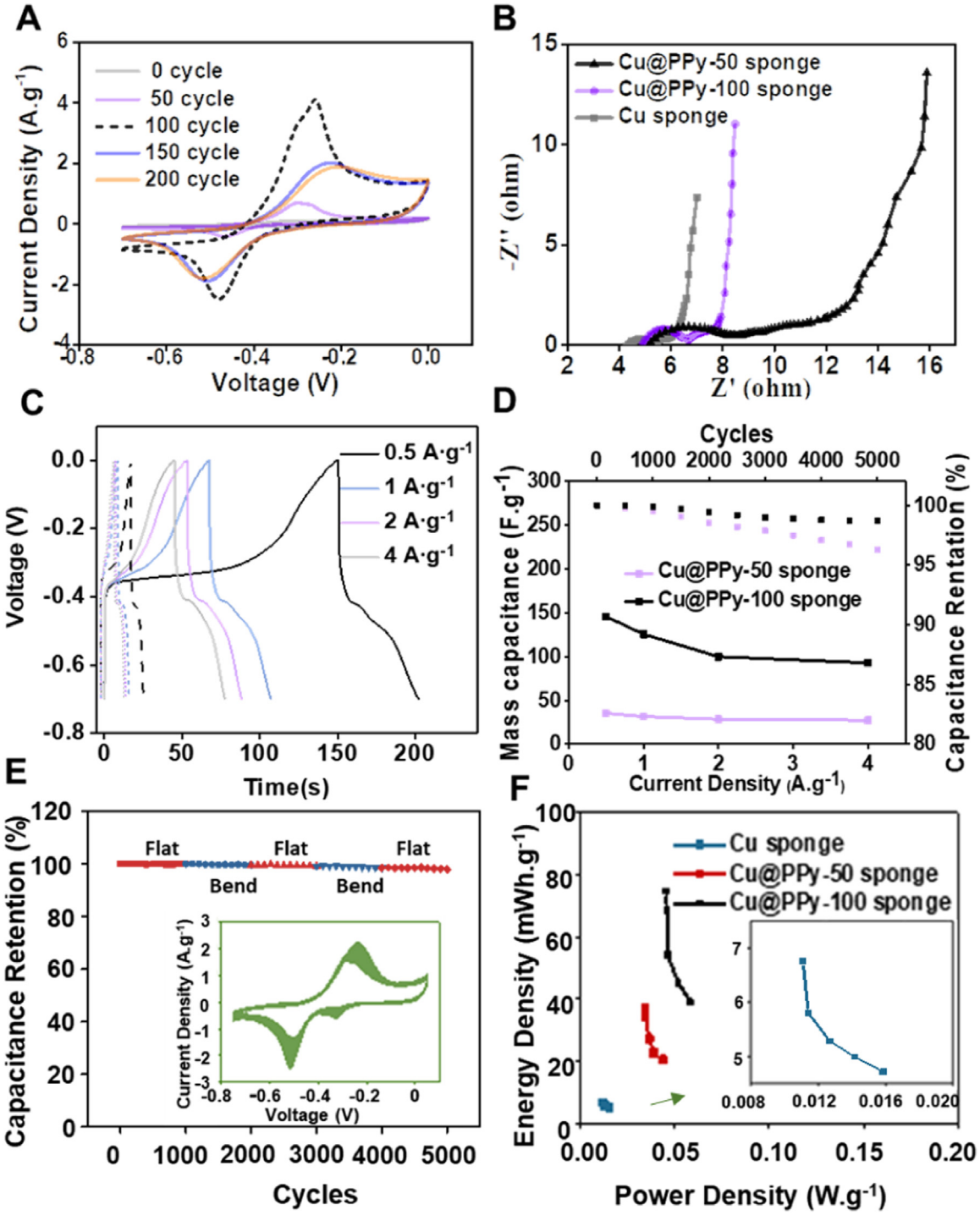

Fig. 3. Electrical measurement in KOH solution. (A) CV curves for Cu@PPy sponges (0, 50, 100, 150 and 200 cycles) at the scan rates of 0.1 V s^{-1}. (B) Nyquist plot from the electrochemical impedance test for different Cu sponges. (C) GCD curves for a supercapacitor based on Cu@PPy sponge (100 deposition cycles in straight line and 50 deposition cycles in dot line) at different current densities. (D) The mass capacitance of Cu@PPy sponge (50 and 100 cycles) as a function of current density. The cycle stability of Cu@PPy-50 and Cu@PPy-100 were also recorded. (E)Cycling stability of Cu@PPy sponges at 0.1 V s^{-1} in flat and bendable states. Inset is the typical CV curve of Cu@PPy-100 sponge. (F) Ragone plots of Cu-sponge supercapacitors with and without PPy deposition. The inset figure in F is a detail view of Ragone plot for Cu sponge. The abscissa is Power Density (W g^{-1}) and the ordinate is Energy Density (mWh g^{-1}) in the inset.

frequency. The *Rs* were approximately 0.25, 0.75, and 0.85 Ω for Cu sponge, Cu@PPy-100, and Cu@PPy-50, respectively. Additionally, the diameter of the semicircle represents the charge-transfer resistance (*R*ct) for the electrode. The *R*ct of Cu@PPy-100 sponge was about 1.8 Ω, only a little higher than that of the Cu sponge (1.2 Ω) and much lower than that of Cu@PPy-50 sponge (3.2 Ω), demonstrating a good binding of the Cu and PPy. The lines in the low frequency range of Cu sponge and Cu@PPy-100 sponge showed almost perpendicular to the Z′-axis which suggested good capacitive behavior without diffusion limitation, however, the Cu@PPy-50 showed as a tilted line which indicates the difficulty in material diffusion [39]. The internal resistance of the Cu sponges with different deposition cycles of pyrrole were studied in Fig. S5 by using I–V characteristics. The original Cu sponge has a resistance of 87 Ω, the resistance of Cu@PPy-50 sponge is 52 Ω,

while the Cu@PPy-100 sponge has a little resistance of 28 Ω. It illustrated that all the three Cu@PPy sponges have great conductivity, which is consistent with the EIS results. The difference between Cu@PPy-50 and Cu@PPy-100 may be caused by the following reasons. The PPy deposited into the Cu@PPy-50 sponge is insufficient to cover all the sponge surface which forms a discontinuous and weak adhesion layer on the sponge. The bad contact between Cu and PPy leads to the awkward electron transfer and ion transfer. In contrast, the contact problem can be ignored in Cu@PPy-100 because sufficient PPy was deposited on the Cu surface, which forms a continuous and interwoven PPy network all through the sponge. As consequence, the PPy will tightly bonded to the Cu and resulted in the fluent electron transfer. In short, the good match of Cu and PPy will exert synergistic effects on enhancing both conductivity and capacitance of the sponges.

In the following study, Cu@PPy-100 sponge was selected for further study as a flexible electrode material. The Cu@PPy-50 sponge was also performed as a control. Fig. S6A and S6B showed the CV results of Cu@PPy-50 and Cu@PPy-100 sponge at scan rates ranging from 0.05 to 0.8 V s^{-1}, respectively. Both of their CV curves displayed obvious a pair of redox peaks, and a highly symmetrical shape appears upon an increase in the scan rate, which exhibits a typical pseudocapacitive shape. As shown in Fig. S6C, the values of mass capacitances against different scan rates were calculated. It could be seen that as the scan rate decreased, the mass capacitance of the fabricated supercapacitor gradually increased and could achieve maximum mass capacitances of 16.3 F g^{-1} and 141.9 F g^{-1} at a scan rate of 0.8 V s^{-1} for Cu@PPy-50 and Cu@PPy-100 sponges respectively. Furthermore, a good supercapacitor is supposed to supply a high mass capacitance at certain charge-discharge rates (current densities). As shown in Fig. 3C, GCD curves of Cu@PPy-100 and Cu@PPy-50 sponges were also measured at different current densities. Electrode potential changes nonlinearly with time during charging and discharging processes due to the pseudocapacitance nature. The mass capacitances can be directly calculated from the GCD curves and the corresponding results are shown in Fig. 3D. The devices exhibit a maximum mass capacitance of 35.4 F g^{-1} and 145.8 F g^{-1} at a current density of 0.5 A g^{-1} for Cu@PPy-50 and Cu@PPy-100 sponges, respectively. The cycling stability was also recorded in Fig. 3D. With 5000 deposition cycle, the Cu@PPy-50 had 95.7% of its original capacitance while the Cu@PPy-100 remained about 98.3%. Both the CV and GCD measurements confirmed once again that the Cu@PPy-100 is outperformed the Cu@PPy-50 in specific capacitance.

The stability of Cu@PPy-100 sponges was examined. The device retained 92.9% of its original mass capacitance after 5000 cycles measurement under stretch-bending state (Fig. 3E), exhibiting satisfying stable performance. The energy density and power density were calculated based on references [40]. As shown in Fig. 3F, the energy density of the Cu@PPy-100 sponge electrode is 75 mWh g^{-1} at a power density of 0.046 W g^{-1}, which is much higher than that of the Cu@PPy-50 sponge electrode (38 mWh·g-1 at a power density of 0.032 W g^{-1}. In terms of the highly stable output performance, the Cu@PPy-100 sponge electrode has promising applications in flexible and wearable devices, such as electronic energy supplier and wearable medical equipment.

To assess the performance of Cu@PPy as electrode for the all-solid-state symmetric supercapacitor (ASSC), we assembled EDSCs based on Cu@PPy electrodes and KOH-polyvinyl alcohol (PVA) as solid electrolyte and separator, namely Cu@PPy//Cu@PPy. Fig. 4A is the structure diagram of SC device, it showed excellent flexibility by compressed or bent, of SC. The SCs were measured at different scan rate from 100 mV s^{-1} to 1000 mV s^{-1}. The CV curves deviated from a rectangular shape owing to the presence of pseudocapacitance of the porous composite (Fig. 4B). The capacitance of the supercapacitor cell was found to be 117.3 F g^{-1} at a scan rate of 100 mV s^{-1} (as shown in Fig. S7A). GCD curves of SCs were also measured at different current densities and shown in Fig. 4C and S7B. The potential changes nonlinearly with time during charging and discharging processes due to the pseudocapacitance nature. The corresponding equivalent circuit is provided in the inset of Fig. 4D and the mass capacitance at 0.5 mA g^{-1} was determined to be 164 F g^{-1}, which remains to be 126 F g^{-1} when increasing the current density 20 times up to 10 A g^{-1} (see Fig. 4D). The Ragone plot, which shows the relationship between the power density and energy density, was plotted in Fig. 4E [41–47]. The corresponding statics were listed in Table 1. It can be seen that at the same power density, the Cu@PPy// Cu@PPy SC exhibited a higher energy density than the GF//GF SSC and the MnO_2//PANI SSC. The highest energy density was found to be 0.129 Wh g^{-1} at a power density of 0.123 W g^{-1}

As for energy-storing devices, the capability to withstand harsh bending or deformation is vital important [48]. As a consequence, a series of flexibility tests were performed. The SC could be compressed or bent under pressure and bending stress, respectively. The Cu@PPy// Cu@PPy SC was compressed by 10%, 30% and 50% to its initial height. The CV curves were recorded in order to examine the performance of the sponge in different compressed states (Fig. 4F). It is evident that there was little or no deviation in the CV curves at different deformation. The flexibility of the SC was further studied in different bending states with the bending angles ranging from 0° to 180°. The CV curves were recorded under different bending states. According to Fig. 4G, there are no distinct changes in device capacitance under various bending states, which implied the SCs is flexible and stable as a device. The stable cycling performance of SC was acquired in Fig. 4H. After a series of bending-compress alternative measurement, it achieved a capacitance retention of 98.2% at 100 mV s^{-1} for 5000 cycles. The CV curves during the course of the cycling kept its original shape and showed no significant degradation (Fig. 3H inset).

On the basis of the specific properties of Cu@PPy sponge, such as portable, lightweight, and flexible, we combined the as-fabricated S-TENG with SC to manufacture a self-powered hybrid energy storage suit (Fig. 5A). As shown in Fig. 5B, the hybrid device has five layers: friction layer, electrode layers, and the electrolyte layer. It had a size of 1.5 × 1.5 × 1.7 cm^3 and a weight less than 0.1 g. The hybrid device is flexible and could be compressed as shown in Fig. 5C. Due to the role of (alternating current) AC-to- (direct current) DC converter, bridge rectifier transferred the energy providing by S-TENG into direct current electricity and store it in the SC. We designed an energy supply mode for a light-emitting diode (LED) light, the generic equivalent electrical circuit was depicted in Fig. 5D. The LED light was connected in parallel to the supercapacitor via a switch (as shown in Fig. 5C inset). By human clapping, the TENG converted the mechanical energy into electricity and acted as an energy supply for the SCs. Depending on the clapping frequency range (1–3 Hz), we obtained the voltage response at different frequencies. As shown in Fig. 5E, the charging rate of the SCs increases as the applied frequency increase. The three in series SCs can be charged to 2.4 V within 3059.6 s under 3 Hz, 7315.2 s under 2 Hz, and 16356.5 s under 1 Hz, which demonstrated its fast response due to increased frequency. Fig. 5F shows the V-t curve of the hybrid energy collection and storage when the S-TENG working under a frequency of 3 Hz for several cycles. As the switch was on, the LED light was powered up with charge leakage (Fig. 5F inset), which demonstrated the feasibility and promising of the hybrid energy collection and storage with the sponge TENG. (G-I) is the detail charging process closely associated with (E). They could be divided into three parts. a-b: the voltage remained constant in a relaxed state; b-c: the voltage increased in a compressed state; c-d: the voltage recovered to constant in next relaxed state. By repeated variation between compressed state and relaxed state, the SCs could be charged to 2.4 V.

4. Conclusion

In summary, we demonstrated the successful fabrication of elastic TENG and SC by using Cu@PPy sponges. The Cu@PPy sponge firstly applied to fabricate single electrode TENG. The output of the TENG was optimized by varying the PPy content in the Cu sponge or hybridization of Cu@PPy with PDMS sponge. This work can significantly promote the

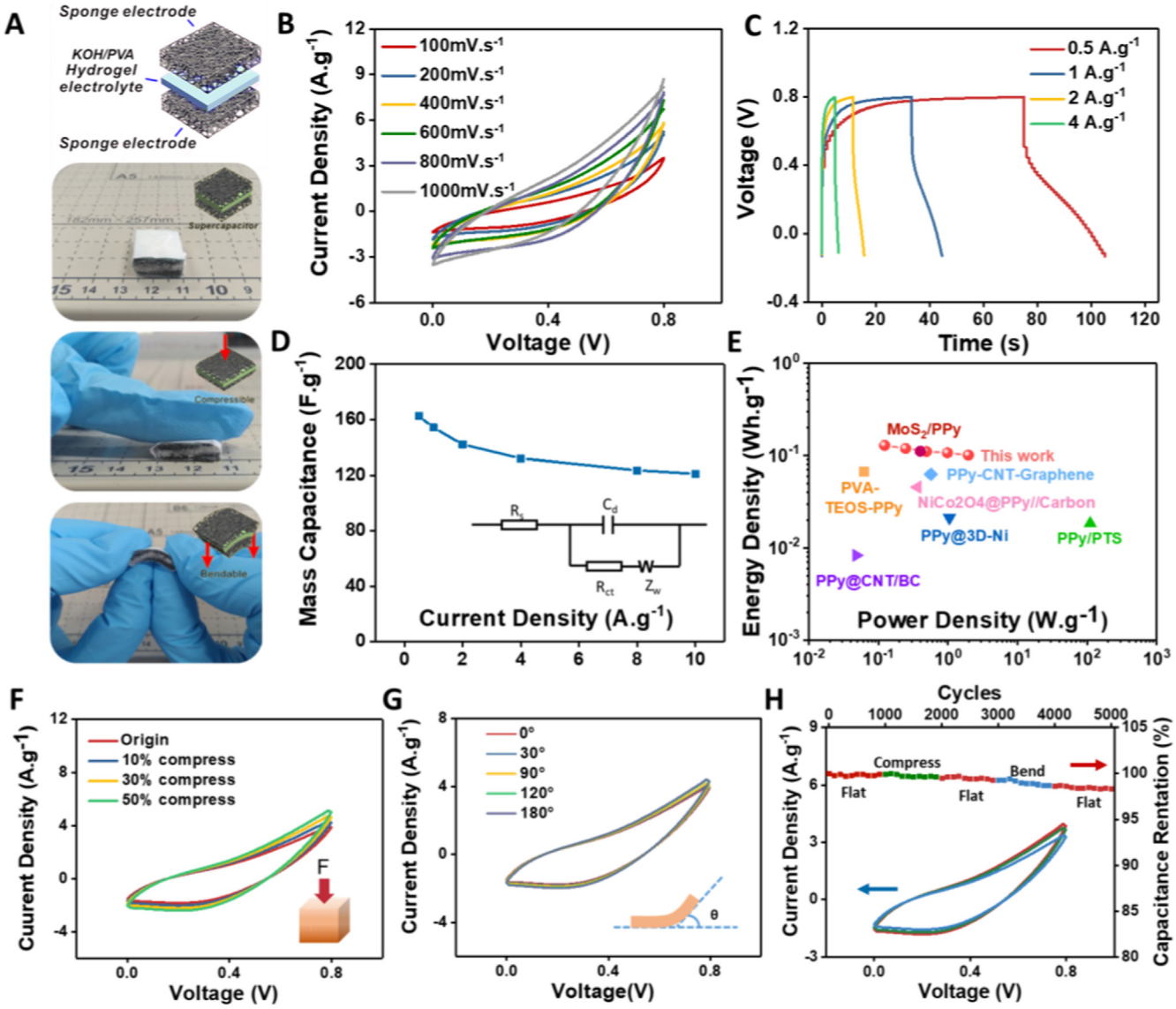

Fig. 4. Electrochemical performance of the all-solid-sate symmetric supercapacitor. (A) Schematic diagram and picture of the SCs with stress or bending force. (B) CV curves of an optimized symmetric supercapacitor at scan rates ranging from 100 to 1000 μmV s^{-1}. (C) Galvanostatic charge-discharge curves at different current densities from 0.5 to 4 A g^{-1} in the potential window of 0.8 V. (D) Mass capacitance variation with different current densities. The inset shows the equivalent circuit diagram of SCs. (E) Ragone plots for the SC with reference values. (F) CV curves for SCs based on Cu@PPy sponges with different deformation. (G) CV curves for SCs with different bending angles. The inset is the diagram of the SCs in bending state. (H) Typical CV curve and cycling stability of symmetric supercapacitor device at 0.1 V s^{-1} under the state of bending and compressed.

Table 1
Typical Results Obtained from PPy-based Flexible Solid-State Supercapacitors.

Supercapacitor	Electrolyte	Power Density (W g^{-1})	Energy Density (Wh g^{-1})	Ref
Cu@PPy	PVA/KOH gel	0.1225	0.12863	This work
Cu@PPy	KOH aq	0.046	0.075	This work
PVA-TEOS-PPy	H_2SO_4	0.0618	0.0672	41
MoS_2/PPy	KCl	0.400	0.111	42
PPy/PTS	HCl	110.9	0.0184	43
PPy@3D-Ni	Na_2SO_4 aq	1.047	0.0212	44
PPy-CNT-Graphene	H_2SO_4	0.566	0.06296	45
$NiCo_2O_4$@PPy//Carbon	–	0.362	0.0456	46
PPy@CNT/BC	PVA-H_3PO_4 gel	0.0478	0.0083	47

understanding of the triboelectricity produced by the TENG from the view of materials and provides a facile way to enhance the performance of TENG by tuning the materials itself. The Cu@PPy supercapacitor achieves high performance and overcomes the insulating problems of sponge by electrochemically interweaving sponge with a conductive polymer PPy. The deposited PPy can efficiently improve the conductivity of sponge and enhance Faradaic processes across the interface. Therefore, such hybrid-structured electrodes take the advantages of

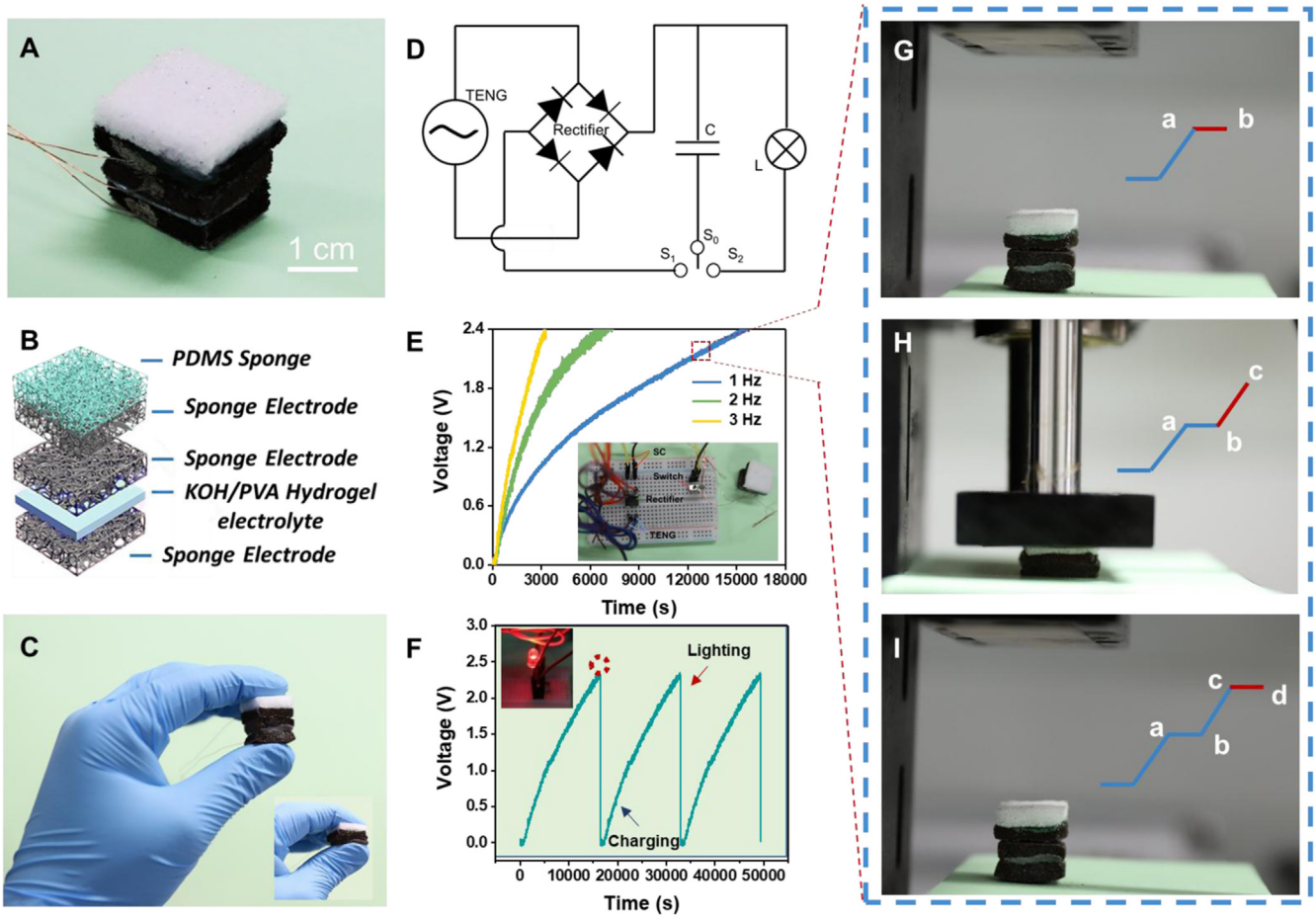

Fig. 5. Fabrication and electrical measurement of hybrid energy collection and storage. (A-C) The diagram of hybrid energy collection and storage. Inset: the devices were compressible. (D-F) Schematic diagram of hybrid device under measurement. (D) Circuit diagram of the energy supply mode. (E) Charging curve of the supercapacitor charged by TENGs at various frequencies. The inset is the diagram of electrical circuit. (F) V–t curve of sponge SC under charging mode and then instantaneously driving a LED. Inset: The red LED was lighted. (G-I) are the detail charging process associated to (E). They could be divided into three parts. a-b: the voltage remained constant in relaxed state; b-c: the voltage increased in compressed state; c-d: the voltage recovered to constant in next relaxed state.

both high EDLC capacitance originated from the internal surface areas of sponge and effective pseudocapacitance generated by PPy. The assembled SC device show excellent flexibility, which has been compressed to 50% of its initial thickness and folded 180°without loss of its performance. Furthermore, for the application of the TENG and the SC, we combined the as-fabricated S-TENG with SC and manufactured a self-powered hybrid energy storage suit. The three in series SCs can be charged to 2.4 V by the S-TENG in about 50 min under 3 Hz and light a LED, which opens great prospects for integrated devices in the future. To close, because of the elasticity, flexibility, and good electric conductivity of the Cu sponge, this porous metal sponge could open new opportunities for developing wearable personal electronics and integrated devices.

Acknowledgements

The authors thank the support of National Key R&D Project from Minister of Science and Technology, China (2016YFA0202703), National Natural Science Foundation of China (No. 61875015, 31571006, 81601629 and 21801019), Beijing Talents Fund (2015000021223ZK21), the Beijing Natural Science Foundation (2182091) and the National Youth Talent Support Program. X. C. Z. acknowledged the Shenzhen Science and Technology Foundation (KQJSCX20170727100240033) for financial support of this work.

Appendix A. Supporting information

Supplementary data associated with this article can be found in the online version at doi:10.1016/j.nanoen.2018.11.093.

References

[1] Z. Niu, W. Zhou, X. Chen, J. Chen, S. Xie, Highly compressible and all-solid-state supercapacitors based on nanostructured composite sponge, Adv. Mater. 27 (2015) 6002–6008.
[2] J. Zhong, Z. Yang, R. Mukherjee, A. Thomas, K. Zhu, P. Sun, J. Lian, H. Zhu, N. Koratkar, Carbon nanotube sponges as conductive networks for supercapacitor devices, Nano Energy 2 (2013) 1025–1030.
[3] K. Xiao, L.X. Ding, G. Liu, H. Chen, S. Wang, H. Wang, Freestanding, hydrophilic nitrogen-doped carbon foams for highly compressible all solid-state supercapacitors, Adv. Mater. 28 (2016) 5997–6002.
[4] W. Chen, R.B. Rakhi, L. Hu, X. Xie, Y. Cui, H.N. Alshareef, High-performance nanostructured supercapacitors on a sponge, Nano Lett. 11 (2011) 5165–5172.
[5] X.J. Li, Z.W. Song, W. Guo, Y. Wang, M. Liang, P. Jiang, W.G. Chu, X.C. Zhao, Y. Liu, Vertically porous Ni(OH) 2 /Ni thin film on carbon cloth for high performance flexible supercapacitors, Mater. Lett. 190 (2017) 20–23.
[6] L. Kou, Z. Liu, T. Huang, B. Zheng, Z. Tian, Z. Deng, C. Gao, Wet-spun, porous, orientational graphene hydrogel films for high-performance supercapacitor electrodes, Nanoscale 7 (2015) 4080.
[7] D.Y. Zhu, S. Handschuh-Wang, X.C. Zhou, Recent progress in fabrication and application of polydimethylsiloxane sponges, J. Mater. Chem. A 5 (2017) 16467–16497.
[8] B. You, J. Jiang, S. Fan, Three-dimensional hierarchically porous all-carbon foams for supercapaci tor, ACS Appl. Mater. Interfaces 6 (2014) 15302–15308.
[9] P. Thurgood, S. Baratchi, C. Szydzik, A. Mitchell, K. Khoshmanesh, Porous PDMS structures for the storage and release of aqueous solutions into fluidic environments, Lab Chip 17 (2017) 2517–2527.

[10] Y. Song, H.T. Chen, Z.M. Su, X.X. Chen, L.M. Miao, J.X. Zhang, X.L. Cheng, H.X. Zhang, Highly compressible integrated supercapacitor-piezoresistance-sensor system with CNT-PDMs sponge for health monitoring, Small 13 (2017) 1702091.

[11] S. Liang, Y. Li, J. Yang, J. Zhang, C. He, Y. Liu, X. Zhou, 3D stretchable, compressible, and highly conductive metal-coated polydimethylsiloxane sponges, Adv. Mater. Technol. 1 (2016) 1600117.

[12] B. Shi, Z. Li, Y. Fan, Implantable energy harvesting devices, Adv. Mater. 30 (2018) 1801511.

[13] Z. Li, H. Feng, Q. Zheng, H. Li, C. Zhao, H. Ouyang, S. Noreen, M. Yu, F. Su, R. Liu, L. Li, Z.L. Wang, Z. Li, Photothermally tunable biodegradation of implantable triboelectric nanogenerators for tissue repairing, Nano Energy 54 (2018) 390–399.

[14] W. Jiang, H. Li, Z. Liu, Z. Li, J.J. Tian, B.J. Shi, Y. Zou, H. Ouyang, C.C. Zhao, L.M. Zhao, R. Sun, H.R. Zheng, Y.B. Fan, Z.L. Wang, Z. Li, Fully bioabsorbable natural-materials-based triboelectric nanogenerators, Adv. Mater. 30 (2018) 1801895.

[15] H.Y. Guo, M.H. Yeh, Y.L. Zi, Z. Wen, J. Chen, G.L. Lin, C.G. Hu, Z.L. Wang, Ultralight cut-paper-based self-charging power unit for self-powered portable electronic and medical systems, ACS Nano 11 (2017) 4475–4482.

[16] C. Yao, X. Yin, Y. Yu, Z. Cai, X. Wang, Chemically functionalized natural cellulose materials for effective triboelectric nanogenerator development, Adv. Funct. Mater. 27 (2017) 1700794.

[17] L.M. Zhao, Q. Zheng, H. Ouyang, H. Li, L. Yan, B.J. Shi, Z. Li, A size-unlimited surface microstructure modification method for achieving high performance triboelectric nanogenerator, Nano Energy 28 (2016) 172–178.

[18] W. Yang, Y. Zhao, X. He, Y. Chen, J. Xu, S. Li, Y. Yang, Y. Jiang, Flexible conducting polymer/reduced graphene oxide films: synthesis, characterization, and electrochemical performance, Nanoscale Res. Lett. 10 (2015) 1–7.

[19] C. Wang, K. Hu, W. Li, H. Wang, H. Li, Y. Zou, C. Zhao, Z. Li, M. Yu, P. Tan, Z. Li, Wearable wire-shaped symmetric supercapacitors based on activated carbon-coated graphite fibers, ACS Appl. Mater. Interfaces 10 (2018) 34302–34310.

[20] F. Yi, J. Wang, X. Wang, S. Niu, S. Li, Q. Liao, Y. Xu, Z. You, Y. Zhang, Z.L. Wang, Stretchable and waterproof self-charging power system for harvesting energy from diverse deformation and powering wearable electronics, ACS Nano 10 (1936) 6519–6525.

[21] H. Chang, G. Wang, A. Yang, X. Tao, X. Liu, Y. Shen, Z. Zheng, A transparent, flexible, low-temperature, and solution-processible graphene composite electrode, Adv. Funct. Mater. 20 (2010) 2893–2902.

[22] M. Ates, S. Caliskan, E. Ozten, Synthesis of ternary polypyrrole/Ag nanoparticle/graphene nanocomposites for symmetric supercapacitor devices, J. Solid State Electr. 22 (2018) 773–784.

[23] H.A.A. Bashid, H.N. Lim, S. Kamaruzaman, S.A. Rashid, R. Yunus, N.M. Huang, C.Y. Yin, M.M. Rahman, M. Altarawneh, Z.T. Jiang, P. Alagarsamy, Electrodeposition of polypyrrole and reduced graphene oxide onto carbon bundle fibre as electrode for supercapacitor, Nanoscale Res. Lett. 12 (2017) 246.

[24] J. Lerner Yardeni, M. Amit, G. Ashkenasy, N. Ashkenasy, Sequence dependent proton conduction in self-assembled peptide nanostructures, Nanoscale 8 (2016) 2358–2366.

[25] G.Z. Chen, M.S.P. Shaffer, D. Coleby, G. Dixon, W. Zhou, D.J. Fray, A.H. Windle, Carbon nanotube and polypyrrole composites: coating and doping, Adv. Mater. 12 (2000) 522–526.

[26] C. Zhou, Y. Zhang, Y. Li, J. Liu, Construction of high-capacitance 3D CoO@polypyrrole nanowire array electrode for aqueous asymmetric supercapacitor, Nano Lett. 13 (2013) 2078–2085.

[27] Y.J. Fan, X.S. Meng, H.Y. Li, S.Y. Kuang, L. Zhang, Y. Wu, Z.L. Wang, G. Zhu, Stretchable porous carbon nanotube-elastomer hybrid nanocomposite for harvesting mechanical energy, Adv. Mater. 29 (2017) 1603115.

[28] S. Liang, Y. Li, Y. Chen, J. Yang, T. Zhu, D. Zhu, C. He, Y. Liu, S. Handschuh-Wang, X. Zhou, Liquid metal sponges for mechanically durable, all-soft, electrical conductors, J. Mater. Chem. C 5 (2017) 1586–1590.

[29] W.H. Guo, T.J. Liu, P. Jiang, Z.J. Zhang, Free-standing porous manganese dioxide/graphene composite films for high performance supercapacitors, J. Colloid Interface Sci. 437 (2015) 304–310.

[30] Z.L. Wang, Triboelectric nanogenerators as new energy technology for self-powered systems and as active mechanical and chemical sensors, ACS Nano 7 (2013) 9533–9557.

[31] U. Khan, T.H. Kim, H. Ryu, W. Seung, S.W. Kim, Graphene tribotronics for electronic skin and touch screen applications, Adv. Mater. 29 (2017) 1603544.

[32] P. Asen, S. Shahrokhian, A high performance supercapacitor based on graphene/polypyrrole/Cu_2O-Cu(OH)(2) ternary nanocomposite coated on nickel foam, J. Phys. Chem. C 121 (2017) 6508–6519.

[33] S.K. Shinde, V.J. Fulari, D.Y. Kim, N.C. Maile, R.R. Koli, H.D. Dhaygude, G.S. Ghodake, Chemical synthesis of flower-like hybrid Cu(OH)2/CuO electrode: application of polyvinyl alcohol and triton X-100 to enhance supercapacitor performance, Colloids Surf. B Biointerfaces 156 (2017) 165–174.

[34] A. Pramanik, S. Maiti, S. Mahanty, Reduced graphene oxide anchored Cu(OH)2 as a high performance electrochemical supercapacitor, Dalton Trans. 44 (2015) 14604–14612.

[35] D. He, G. Wang, G. Liu, H. Suo, C. Zhao, Construction of leaf-like CuO-Cu2O nanocomposites on copper foam for high-performance supercapacitors, Dalton Trans. 46 (2017) 3318–3324.

[36] A. Galal, H.K. Hassan, T. Jacob, N.F. Atta, Enhancing the specific capacitance of SrRuO3 and reduced graphene oxide in $NaNO_3$, H_3PO_4 and KOH electrolytes, Electrochim. Acta 260 (2018) 738–747.

[37] O. Fasakin, J.K. Dangbegnon, D.Y. Momodu, M.J. Madito, K.O. Oyedotun, M.A. Eleruja, N. Manyala, Synthesis and characterization of porous carbon derived from activated banana peels with hierarchical porosity for improved electrochemical performance, Electrochim. Acta 262 (2018) 187–196.

[38] Z. Guo, Q. Zhou, Z. Wu, Z. Zhang, W. Zhang, Y. Zhang, L. Li, Z. Cao, H. Wang, Y. Gao, Nitrogen-doped carbon based on peptides of hair as electrode materials for surpercapacitors, Electrochim. Acta 113 (2013) 620–627.

[39] Q. Wang, P. Pechy, S.M. Zakeeruddin, I. Exnar, M. Gratzel, Novel electrolytes for $Li_4Ti_5O_{12}$-based high power lithium ion batteries with nitrile solvents, J. Power Sources 146 (2005) 813–816.

[40] K. Ghosh, C.Y. Yue, M.M. Sk, R.K. Jena, Development of 3D urchin-shaped coaxial manganese dioxide@polyaniline (MnO_2@PANI) composite and self-assembled 3D pillared graphene foam for asymmetric all-solid-state flexible supercapacitor application, ACS Appl. Mater. Interfaces 9 (2017) 15350–15363.

[41] A.I. Torvi, B.B. Munavalli, S.R. Naik, M.Y. Karidurаganavar, Scalable fabrication of a flexible interdigital micro-supercapacitor device by in-situ polymerization of pyrrole into hybrid PVA-TEOS membrane, Electrochim. Acta 282 (2018) 469–479.

[42] D. Sarmah, A. Kumar, Layer-by-layer self-assembly of ternary MoS2 -rGO@PPyNTs nanocomposites for high performance supercapacitor electrode, Synth. Met. 243 (2018) 75–89.

[43] J. Wang, Y. Xu, J. Wang, X. Du, Toward a high specific power and high stability polypyrrole supercapacitors, Synth. Met. 161 (2011) 1141–1144.

[44] G.F. Chen, Y.Z. Su, P.Y. Kuang, Z.Q. Liu, D.Y. Chen, X. Wu, N. Li, S.Z. Qiao, Polypyrrole shell@3D-Ni metal core structured electrodes for high-performance supercapacitors, Chem.-Eur. J. 21 (2015) 4614–4621.

[45] A. Aphale, K. Maisuria, M.K. Mahapatra, A. Santiago, P. Singh, P. Patra, Hybrid electrodes by in-situ integration of graphene and carbon-nanotubes in polypyrrole for supercapacitors, Sci. Rep. 5 (2015) 14445.

[46] S. Liu, C. An, X. Chang, H. Guo, L. Zang, Y. Wang, H. Yuan, L. Jiao, Optimized core–shell polypyrrole-coated NiCo2O4 nanowires as binder-free electrode for high-energy and durable aqueous asymmetric supercapacitor, J. Mater. Sci. 53 (2018) 2658–2668.

[47] J. Yao, P. Ji, N. Sheng, F. Guan, M. Zhang, B. Wang, S. Chen, H. Wang, Hierarchical core-sheath polypyrrole@carbon nanotube/bacterial cellulose macrofibers with high electrochemical performance for all-solid-state supercapacitors, Electrochim. Acta 283 (2018) 1578–1588.

[48] H.B. Yao, J. Ge, C.F. Wang, X. Wang, W. Hu, Z.J. Zheng, Y. Ni, S.H. Yu, A flexible and highly pressure-sensitive graphene-polyurethane sponge based on fractured microstructure design, Adv. Mater. 25 (2013) 6692–6698.